Chapter 4

Spectroscopy

4.1 Observations

The spectroscopic observations for this work were obtained during 8 observing runs with the Hale 5m telescope of the Palomar Observatory. During all runs the red camera of the Double Spectrograph (Oke & Gunn 1982) was used with a 1200 lines/mm grating, to produce spectra with a dispersion of approximately 0.82 Å per pixel (except in runs 7 and 8, when a different CCD chip was mounted on the camera, and the dispersion was approximately 0.66 Å per pixel). This resulted in a spectral coverage of approximately 600 Å, from 5000 to 5600 Å, centered on the Mg Ib lines at $\lambda \sim 5175$. The spectral resolution (measured both from the width of the calibration lamps lines, and from the width of the peak in the autocorrelation function of the spectrum of velocity standard stars) was approximately 2.2 Å for all runs, which is equivalent to a velocity resolution of 129 km s^{-1}(at 5300 Å). All observations were obtained with a 2 arcsec wide slit (the length of the slit is 128 arcsec). The slit orientation was in the East-West direction, unless a close pair of galaxies could be observed at once with the proper slit orientation. Table 4.1 summarizes these observing runs, and gives some parameters of the relative instrumental set-ups. Integration times varied between 10 and 90 minutes, depending on the brightness of the galaxy. The median integration time was 30 minutes. He-Ne-Ar lamp spectra were obtained before and after each galaxy observation, to provide wavelength calibration.

Spectra for 212 galaxies were obtained. Galaxies to be observed were selected to satisfy the following criteria: redshift and angular distance from the cluster center in the interval appropriate for the given cluster (see Chapter 2 for a discussion on cluster membership), morphological type E, S0 or S0a. The observed samples are roughly complete down to a magnitude $m_{pg} \simeq 15.2$, and the degree of completeness for fainter magnitudes changes greatly from cluster to cluster, the Coma and A2634 clusters being the only ones where observations reach significantly fainter magnitudes. Since these are also the farthest clusters in the sample, the absolute luminosity limit is approximately the same in all clusters. Late G and early K type giant stars were observed to serve as templates for radial velocity and velocity dispersion determinations. To maximize the signal-to-noise ratio in these template spectra, the star observations were obtained with 30-120 sec integrations, while trailing the star along the slit. This allowed to spread the light on a large area of the CCD chip without saturating the image.

Table 4.1 Spectroscopic observing runs

	Runs 1–6	Runs 7–8
Telescope	Palomar 5m	Palomar 5m
Instrument	DS-red camera	DS-red camera
CCD	TI 305 #8	Tek1024
Pixels	800 x 300	1024 x 300
Read-out noise	11 e^-	7.5 e^-
Gain	1.7 e^-/DU	2.0 e^-/DU
Spatial scale	0.61 ″/pixel	0.46 ″/pixel
Slit aperture	2 arcsec	2 arcsec
Grating	1200 l/mm	1200 l/mm
Dispersion	0.82 Å/pixel	0.64 Å/pixel
Spectr. resol.	2.2 Å(129 km/s)	2.2 Å(129 km/s)
Wavelength cover.	4960-5620 Å	4960-5660 Å

	Run 1	Run 2	Run 3
Dates	Sep 23-26 1992	Sep 17-20 1993	Mar 3-6 1994
Nights used	2	4	3
Nr. of galaxies	16	84	35

	Run 4	Run 5	Run 6
Dates	Apr. 28-29 1994	Sep. 6-12 1994	Aug. 23-25 1995
Nights used	1	7	3
Nr. of galaxies	6	112	28

	Run 7	Run 8
Dates	Mar 19-20 1996	Sep 20 1996
Nights used	1	1
Nr. of galaxies	5	8

4.2 Basic reduction and wavelength calibration

The data-reduction process has been performed entirely using standard IRAF procedures. All frames have been bias-subtracted, to remove the signal offset introduced by the read-out electronics, and then flat-fielded, to remove the pixel-to-pixel sensitivity variations. Dome flats, obtained pointing the telescope at a white, uniformly illuminated spot inside the dome, have been used for this purpose. The number of pixels affected by "cosmic rays hits" was small in all the frames, so that the problem of removing this contamination has been easily solved.

Wavelength calibration has been performed in a two-step process. First, the He-Ne-Ar lamp spectra frames obtained before and after each galaxy spectrum have been used to obtain a two-dimensional dispersion solution, where a wavelength value is assigned to each pixel in the CCD frame. Typically 12-14 spectral lines, spread uniformly over the entire wavelength range, have been used in the fit. The rms deviations between fitted and true wavelength are of the order of 0.06–0.1 Å in the central portion of the frames (where the galaxy spectra are positioned), and increase up to 0.25 Å at the edges of the frame, due to the camera astigmatism and to focusing problems caused by the less than perfect flatness of the CCD chip. Single line deviations from the best fit solutions are always less than 0.3 Å. An uncertainty in the wavelength calibration of 0.1 Å at 5300 Å translates into a velocity uncertainty of 5.6 km s^{-1}. The CCD chip used for runs 7 and 8 does not have these focusing problems, and therefore the rms uncertainty in the calibration of the spectra obtained in that run is of the order of 0.08 Å, uniformly across the entire frame. The galaxy spectra frames have been then transformed to linear dispersion using the two-dimensional dispersion solutions, and distortions have been corrected, so that all pixels in one row of the CCD frame are characterized by the same wavelength. Finally the two strong night-sky lines at 5460.7 Å (Hg) and 5577.4 Å (OI) have been used to check the absolute wavelength calibration. The 1-σ dispersion in the measured wavelengths of these lines is approximately 0.08 Å. A small fraction (2-3%) of the frames showed large deviations ($> 4\sigma$) in the wavelength measured for the two sky lines. For these cases the original dispersion solution has been rigidly shifted to bring the two lines into agreement with their expected wavelengths.

An independent check on the wavelength calibration has been done using the velocity standard star spectra. Radial velocities have been measured repeatedly using all star spectra obtained in the different runs. Using in turn one star as velocity standard and all others as unknown, radial velocities have been derived, to be compared with the known radial velocity of each star. The dispersion in the differences between the known and the measured velocities is between 6.0 and 8.5 km s^{-1}, when spectra obtained during a single run only are considered, and approximately 9 km $s^{-1}$when spectra from all runs are considered. This result is in good agreement with the calibration uncertainty derived from the sky lines measurements. Therefore 9 km $s^{-1}$is an estimate of the maximum accuracy we can achieve with this spectroscopic data-set, both in terms of radial velocities, and of velocity dispersions.

The final one-dimensional galaxy spectra have been extracted from the relative frames using a 6 arcsec wide window, centered on the peak of the galaxy continuum. This, combined with the 2 arcsec slit aperture, provides a final effective aperture of 6 x 2 arcsec for all the galaxy observations. The stellar templates have been obtained averaging the signal over 20–30 pixels in the spatial dimension at all wavelengths, to produce spectra with a signal to noise ratio greater than 200. Because more than half of the spectroscopic observations were obtained in non-photometric conditions, no attempt has been made to obtain a flux-calibration for any of the derived spectra.

4.3 Determination of the spectroscopic parameters

The stellar velocity dispersion σ is the most difficult parameter to derive, among those that enter the FP relation. Even the strongest absorption lines in galaxy spectra (the Na D lines, the Ca H and K lines, the Mg Ib lines) require a spectrum with high signal-to-noise ratio (i.e. many hundred counts per pixel in the spectral continuum around the lines) before their shape can be accurately determined. This fact, and the moderately high dispersion necessary to resolve the lines, result in long integration time requirements for spectroscopic observations geared at velocity dispersion measurements, even with large (4 meter class) telescopes. Another complication for velocity dispersion determinations is caused by the partial degeneracy between line width (used to measure σ) and line strength in determining the global line shape (both are unknown quantities in the problem).

During the last twenty years a number of methods have been developed to perform velocity dispersion measurements as objectively as possible (Sargent *et al.* 1977; Tonry & Davis 1979; Franx *et al.* 1989; Bender 1990). These methods are all based on a "comparison" between the spectrum of the galaxy whose velocity dispersion is to be determined, and a fiducial spectral template. This can be either the spectrum of an appropriate star, with spectral lines unresolved at the spectral resolution being used, or a high signal-to-noise spectrum of a galaxy with known velocity dispersion. There are small but in principle significant differences among these methods, but in practice all methods seem to give results in good relative agreement, when applied to spectra with high signal-to-noise ratio, making the choice of one particular method a non-critical issue.

In this work, all quantitative measurements on the spectra have been obtained using the cross-correlation technique of Tonry & Davis (1979), implemented in the IRAF task *fxcor*. The basic assumption behind this and other similar methods is that the spectrum of an elliptical galaxy (and also of the bulge of a disk galaxy) is well approximated by the spectrum of its most luminous stars (K0–K1 giants), modified only by the effects of the stellar motions inside the galaxy. Since these motions introduce just a Doppler shift in the stellar spectra, the galaxy spectrum is given by the convolution of the spectrum of a K giant star with the line of sight stellar velocities distribution (LOSVD). Therefore the LOSVD can be obtained with a deconvolution process from the galaxy spectrum and a suitable stellar template.

In practice, given that cross-correlation and convolution are two related operators, Tonry & Davis use the cross-correlation as a computational tool to derive the LOSVD. The entire procedure is performed using Fourier transforms, because the Fourier transform of a convolution, or of a cross-correlation reduces to a product between individual functions' transforms. Before computing the Fourier transforms and the cross-correlation function, all spectra have been continuum-subtracted, normalized, end-masked with a cosine bell function, and re-binned to a logarithmic wavelength scale.

4.3.1 The Effect of the Noise

Because of the limited signal-to-noise ratio of the spectra being analyzed, and also to facilitate comparisons with other studies, we have constrained the deconvolution procedure by assuming the LOSVD to be Gaussian, and therefore characterized by two parameters only: a mean redshift z and a velocity dispersion σ. The reliability of this method has been tested using simulations with synthetic spectra. Stellar templates have been broadened with Gaussian profiles of known width to simulate a large range of velocity dispersions, and noise has been added to the resulting spectra, to reproduce the signal-to-noise characteristic of the galaxy spectra. Then velocity dispersions have been measured using the original stellar spectrum as a template.

The aforementioned tests show that *fxcor* produces an overestimate of the velocity dispersion, at the 4-5% level, while no bias is present in the measurement of radial velocities. The raw measurements have been therefore corrected to remove this effect. The final velocity dispersion measurements have been obtained by averaging the determinations obtained with five different stellar templates, of spectral types between G9 and K2. If the true LOSVD is approximately Gaussian, then the statistical uncertainty with which the velocity dispersion is obtained is a function of the signal-to-noise ratio of the galaxy spectrum only, since the signal-to-noise ratio (S/N) in the template spectrum is many times higher than that of the galaxy spectrum (see Tonry & Davis 1979 for details). An estimate of the amplitude of this uncertainty was obtained using synthetic spectra with added noise. It was found that a good approximation to the value of the uncertainty is given by the relation $\epsilon_{\log\sigma} \simeq 1.1/(S/N)$. The mean uncertainty on the radial velocity determination is 13 km s^{-1}, and on the velocity dispersion is 5.1%.

4.3.2 The Effect of Rotation

Galaxy one-dimensional spectra were extracted using a 6 arcsec aperture, which can bracket a fairly large portion of the target galaxy, especially for more distant clusters. Therefore galaxy rotation, if present, can contribute some broadening of the spectral lines and bias the velocity dispersion measurements. We thus use the galaxy two-dimensional spectra to estimate the galaxy rotation velocity, and gauge whether a correction of the velocity dispersion measurements is necessary. A 5 point rotation curve within the 6 arcsec aperture (10 pixels) has been obtained for each galaxy, using 5 one-dimensional spectra, extracted using 2-pixel wide apertures positioned side by side. Using the cross-correlation method, individual mean velocities can be obtained for the 5 spectra. The differences in the radial velocities measured between each one of the four lateral spectra and the one measured in the central 2 pixels define the projection of the galaxy rotation curve along the slit.

The contribution of a given rotation to the broadening of the spectral lines has been estimated using a very simple model. A galaxy spectrum has been simulated combining 5 copies of a stellar template, broadened with a Gaussian of fixed width, and shifted to reproduce the 5 velocities in the rotation curve. The weights used in the combination have been derived from the relative intensities in the continuum of the 5 one-dimensional galaxy spectra used to obtain the rotation curve. The comparison of the velocity dispersion in the simulated spectrum with the one used to broaden the stellar template spectra provides an estimate of the amount of broadening due to the rotation.

Given the accuracy with which radial velocities can be measured, and the small number of points used to define the rotation curve, rotation velocities smaller than $\simeq$20 km s^{-1} cannot be reliably measured. Within the sample presented here, 75 galaxies do not show detectable rotation. The remaining 200 have a median rotation velocity of 40 km s^{-1}, with the largest measured velocity being 130 km s^{-1}. This rotation is responsible for an average broadening of the LOSVD of $\simeq$4%, with a maximum of $\simeq$9% for the largest rotation velocities.

4.3.3 Aperture Correction

Because of radial gradients in the stellar velocity dispersion within early-type galaxies, the velocity dispersion measured in a given galaxy depends on the size of the aperture that is used to extract its spectrum. When spectra are obtained with a fixed aperture size (in arcseconds), this aperture covers regions of different physical size (in kiloparsec) on galaxies at different distances, and this produces biased velocity dispersion measurements. Therefore fixed aperture measurements must be corrected to a standard, distance independent, aperture size. Here all measurements are corrected to the value one would obtain for a galaxy at the distance of the Coma cluster, using the relation derived by Jørgensen, Franx & Kjærgaard (1996)

$$\log \frac{\sigma_{ap}}{\sigma_{norm}} = -0.04 \ \log \frac{r_{ap}}{r_{norm}} = -0.04 \ \log \frac{d}{d_{Coma}} \tag{4.1}$$

where σ_{ap} and σ_{norm} are the measured and corrected velocity dispersion, r_{ap} and r_{norm} are the projected angular size of a given length at the distance of the observed galaxy and at the reference distance used for the normalization, and d and d_{Coma} are the distance of the observed galaxy and of the Coma cluster.

The results of the spectroscopic observations are summarized in Table A.3 in the appendix. The table is organized as follows:
Col. 1: Galaxy name, as in Table A.1.
Col. 2: Radial heliocentric velocity, in km s^{-1}.
Col. 3: Measured stellar velocity dispersion, in km s^{-1}.
Col. 4: Measured rotation velocity, in km s^{-1}.
Col. 5: Velocity dispersion, in km s^{-1}, corrected for galaxy rotation.
Col. 6: Logarithm of the rotation-corrected velocity dispersion.
Col. 7: Uncertainty on the logarithm of the velocity dispersion.
Col. 8: Aperture-corrected logarithm of the velocity dispersion.
Col. 9: A reference code indicates if other velocity dispersion measurements were available in the literature, and their source. If an asterisk appears in this column, special comments on the object are included at the foot of the table.

4.4 Data taken from the literature

A significant number of velocity dispersion measurements used in this work has been taken from Dressler (1987), Davies *et al.* (1987) and Faber *et al.* (1989), and from Lucey

et al. (1991a,b). The instrumental set-up used in those studies, and the methods used to measure the velocity dispersions, are quite similar to the ones used in this work. It is therefore possible to use those measurements directly alongside the new measurements presented here, in building a FP relation (see next section for a comparison of the different measurements). Table A.4 in the appendix lists the 118 measurements taken from the literature, and is organized as follows:
Col. 1: Galaxy name, as in Table A.1.
Col. 2: Radial heliocentric velocity, in km s^{-1}.
Col. 3: Stellar velocity dispersion, in km s^{-1}.
Col. 4: Logarithm of the velocity dispersion.
Col. 5: Quoted mean uncertainty on the logarithm of the velocity dispersion.
Col. 6: Aperture-corrected logarithm of the velocity dispersion.
Col. 7: A reference code indicates the source of the velocity dispersion measurement. If an asterisk appears in this column, special comments on the object are included at the foot of the table.

4.5 Internal and external comparison

Repeated observations of a small fraction of the galaxies listed in Table A.3 provide the opportunity to evaluate the internal consistency of the spectroscopic measurements. Unlike the case of the photometric observations, the number of repeated observations is rather small, because the spectroscopic observations are very expensive in terms of telescope time. In total, 18 pairs of observations are available for an internal comparison. Table 4.2 lists the results of the comparison of radial velocity and velocity dispersion (see also Figure 4.1). Again, the mean statistical uncertainties associated with the derivation of those parameters is included in the Table, multiplied by a $\sqrt{2}$ factor to allow a direct comparison with the rms scatter in the observations. The rms scatter in the radial velocity comparison is surprisingly large (34 km s^{-1}), but it is mostly due to just 3 galaxies. After removing these 3 extreme cases the scatter is reduced to 17 km s^{-1}, in agreement with the statistical uncertainties on the radial velocity determinations. Unfortunately with such small number statistics it is difficult to decide whether these 3 objects are truly outliers, or if the distribution of velocity differences is actually broader than expected.

The comparison of the velocity dispersions shows that the accuracy of the dispersion determinations for very low velocity dispersion objects ($\sigma < 90$km s^{-1}) is significantly lower than that of higher velocity dispersion. The rms scatter measured for the 5 low velocity dispersion objects is in fact more than twice as large as the one measured for the remaining 13 objects. Overall, there is fair agreement between the expected uncertainties and the observed dispersion in the measurements.

The absolute consistency of the velocity dispersion measurements is evaluated through a comparison with measurements taken from the literature. There are 38 galaxies among those listed in Table A.3 that were also observed by Dressler (1987), Davies *et al.* (1987) and Faber *et al.* (1989), and by Lucey *et al.* (1991a,b). The results of such a comparison are presented in Table 4.3 and in Figure 4.2. It is clear that there is good agreement with the long-slit observations of Dressler (1987), Davies *et al.* (1987), Faber *et al.* (1989), and Lucey *et al.* (1991b), while a significant discrepancy is present when the

Table 4.2 Spectroscopy internal comparison

Parameter	N	mean difference	rms scatter	mean uncertainty
V_{hel} (all)	18	0.83	34	18
V_{hel} (3 most discr. excluded)	15	-2.2	17	18
$\log\sigma$ (all)	18	0.0002	0.063	0.031
$\log\sigma$ ($\sigma > 90$ km s^{-1})	13	-0.0005	0.043	0.031
$\log\sigma$ ($\sigma < 90$ km s^{-1})	5	0.0021	0.107	0.031

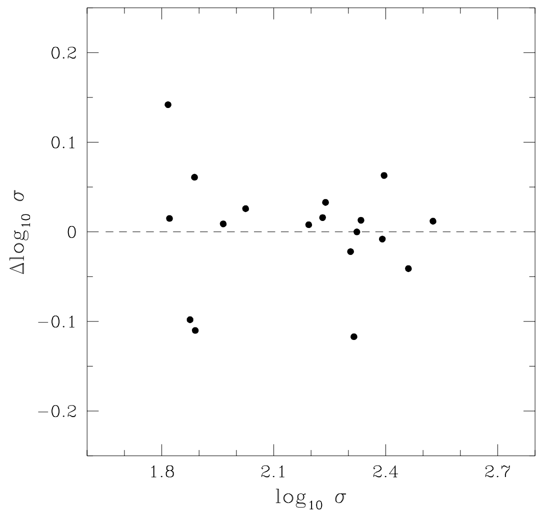

Figure 4.1 Internal comparison of the velocity dispersion measurements.

Table 4.3 Spectroscopy external comparison

Parameter	N	mean difference	rms scatter
$\log\sigma$ (all)	38	-0.012	0.058
$\log\sigma$ (L34[a] excluded)	31	-0.0003	0.057
$\log\sigma$ (L34[a] only)	7	-0.060	0.039

[a] Lucey et al. (1991a): A2634 data

A2634 multifiber observations of Lucey *et al.* (1991a) are considered (see also Scodeggio, Giovanelli & Haynes 1997a). Lucey *et al.* (1991a) velocity dispersions appear to be overestimated by ≃14%. This is also confirmed by new measurements in this cluster by Lucey and coworkers (Guzmán 1996). When these 7 measurements are removed from the comparison, the velocity dispersion scale used here appears to be in excellent agreement with that of the other studies. We therefore have decided to merge all measurements in a single data-base of velocity dispersions, simply applying a 14% correction to the 7 Lucey *et al.* (1991a) measurements.

4.6 On the cross-correlation method

A number of very similar methods have been proposed during the last twenty years, to measure the velocity dispersion inside a galaxy from the observed broadening of the absorption lines in the galaxy spectrum (Simkin 1974; Sargent *et al.* 1977; Tonry & Davis 1979; Dressler 1979; Franx *et al.* 1989; Bender 1990). All these methods assume that the spectrum of an elliptical galaxy (and also of the bulge of a disk galaxy) is well approximated by the spectrum of its most luminous stars (K0–K1 giants), modified only by the effects of the stellar motions inside the galaxy. Since these motions introduce just a Doppler shift in the stellar spectra, the galaxy spectrum is given by the convolution of the spectrum of a K giant star with the line of sight stellar velocities distribution (LOSVD). Therefore the LOSVD can be obtained with a deconvolution process from the galaxy spectrum and a suitable stellar template.

In its simplest version, the method works in this way: if we denote with $G(x)$ and $S(x)$ the galaxy and stellar template spectrum, respectively, where the independent variable x represents the wavelength, in logarithmic scale, then the two spectra are related via the relation

$$G(x) = \alpha S(x) * B(x-\delta) \tag{4.2}$$

where $B(x-\delta)$ is the Doppler broadening function, shifted in wavelength by an amount δ, corresponding to the galaxy redshift, and $*$ means convolution product. The coefficient α is just a normalization constant. In Fourier space this convolution product becomes a

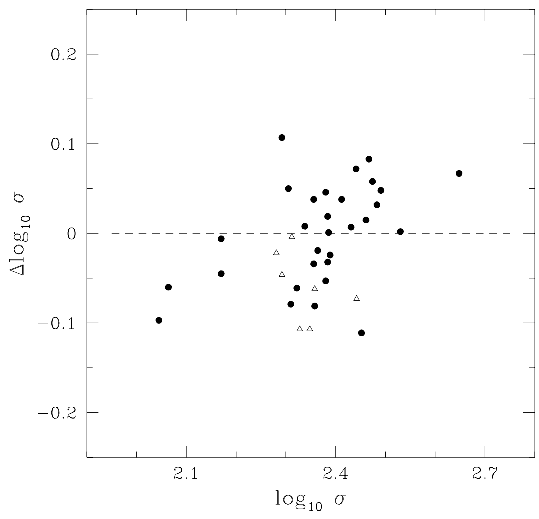

Figure 4.2 External comparison of the velocity dispersion measurements. Empty symbols identify the comparison with the measurements of Lucey et al. 1991a, that are believed to be systematically too large (see text).

normal product:

$$\tilde{G}(k) = \alpha \tilde{S}(k)\tilde{B}(k)exp(ik\delta) \tag{4.3}$$

and the broadening function can therefore be obtained from the ratio of the galaxy and stellar template spectra

$$\tilde{B}(k) = \frac{\tilde{G}(k)}{\tilde{S}(k)} exp(ik\delta) \tag{4.4}$$

(Fourier quotient technique, Sargent *et al.* 1977). However this simple technique has a rather severe problem in the noise associated with real data, that can introduce poles in the G/S ratio (i.e. points where $\tilde{S}(k)$ goes to zero).

To avoid this problem Tonry & Davis (1979) proposed a modified version of the technique (cross-correlation technique), where the broadening function is obtained from a chi-squared minimization

$$\chi^2(\alpha, \delta, B) = \sum_x \left[\alpha S(x) * B(x-\delta) - G(x)\right]^2 \tag{4.5}$$

$$\sim \alpha^2 \sum_x \left[S(x) * B(x-\delta)\right]^2 - 2\alpha \sum_x \left[S(x) * B(x-\delta) G(x)\right] + \sum_x \left[G(x)\right]^2 \tag{4.6}$$

The parameter α can be obtained minimizing this chi-squared function with respect to alpha itself. When this value is substituted back into equation (4.6) one gets

$$\chi^2(\alpha_{min}, \delta, B) = N\sigma_g^2 \left(1 - \frac{\sigma_s^2}{\sigma_{sb}^2} \left[C(x) * B(\delta)\right]^2\right) \tag{4.7}$$

where $\sigma_g^2 = 1/N \sum_x G(x)^2$ and $\sigma_s^2 = 1/N \sum_x S(x)^2$ are the rms values of the galaxy and stellar template spectrum, $\sigma_{sb}^2 = 1/N \sum_x [S * B]^2$ is the rms of the broadened stellar template, and $C(x) = 1/N \sum_y G(y)S(y-x)$ is the cross-correlation of the galaxy and stellar template spectra. Therefore the minimization of χ^2 is equivalent to the maximization of the convolution

$$\frac{1}{\sigma_{sb}}\left[C(x) * B(\delta)\right] \tag{4.8}$$

between the cross-correlation function and the broadening function. This maximization is once again performed in Fourier space, to take advantage of the convolution product becoming an ordinary product in the Fourier domain.